SCIENTIFIC REPORTS

OPEN

A heralded and error-rejecting three-photon hyper-parallel quantum gate through cavity-assisted interactions

Ji-Zhen Liu, Hai-Rui Wei & Ning-Yang Chen

Hyper-parallel quantum computation is a promising and fruitful area of research with its high capacity and low loss rate characters. In this paper, we propose a heralded, compact, scalable, and deterministic error-rejecting scheme for implementing three-photon hyper-parallel Toffoli gate simultaneously acting on polarization and spatial degrees of freedom. It is a practical and unity gate without strong coupling strength limitations, since the undesired performances caused by the side leakage and the limited coupling strength are detected by the single-photon detectors. The success of our proposal can be heralded by the detectors, and the efficiency can be further improved by repeating the operation processes when the detectors are clicked. The evaluation of gate performance with experimental parameters shows that it is feasible with current experimental technology.

Exploiting quantum mechanics and the superposition principle, quantum computers outperform classical computers on certain computationally demanding problems like searching databases[1,2], factoring large integers[3], quantum simulation and modeling[4]. Nowadays, much research has been done in traditional parallel quantum computing[5,6]. Recently, hyper-parallel quantum information processing (QIP) has attracted growing interest[7,8] duo to its high capacity encoding, low loss rate, increased security of the communication, and hyper-parallel computing. Quantum conditional gates[9,10] or similar logic operations[11] are the key components for quantum computing[12]. Moreover, multi-qubit conditional gates are very useful in quantum error correction[13], quantum algorithm[14], fault-tolerant quantum circuits[15], and quantum network[16]. Controlled-NOT (CNOT) gate is the most popular universal conditional gate[12], i.e., supplemented with one-qubit unitary gates one can perform any quantum computing[9]. Implementation of multi-qubit Toffoli gate[17] or Fredkin gate[18] is an important milestone for scalable quantum computer. Therefore, investigation of the hyper-parallel multi-qubit gate will open an avenue in scalable hyper-parallel quantum information processing.

Impressive theoretical and experimental progress has been made and realized in parallel and hyper-parallel CNOT, Toffoli, and Fredkin gates in various physical systems today[19–24]. Photon has been recognized as one of the most popular and promising candidates for parallel and especially hyper-parallel quantum information processing thanks to its available single-qubit operations, low decoherence, faithful transmission of information, and many available qubit-like degrees of freedom (DOFs)[25]. However, scalability is the main objective for optical computing with current technology due to weak interaction in single-photon level. One approach for achieving this goal is to employ linear optics and photon detectors, and only probabilistic gates with a maximal probability of success 3/4 have been explored[19]. Another approach is to employ distributed or modular architecture. The emitted solid-state platform can be efficiently configured to mediate photon-photon or spin-spin interaction. Nowadays, the efficient emitted platforms have ranged from natural atoms[26] or Rydbery atom ensembles[27] to artificial atoms such as QD[28,29], diamond nitrogen vacancy defect center[30], and superconductor[21]. The interactions between individual photons and stationary qubits are generally weak, and cavity quantum electrodynamics (QED) are usually exploited to overcome this challenge by confining photons for a long time in a small region[31].

Numerous theoretical and experimental achievements about the emitter-based gates have been reported[32,33]. Recently, quantum dot (QD) inside a microcavity has received much attention because of its μs coherence time[34,35], fast QD spin manipulation[36], scalability, and optical property. In 2008, Hu *et al.*[28,29] proposed an interesting QD-based emitter, a self-assembled In(Ga)AS QD or GaAs interface QD confined in a resonant microcavity,

School of Mathematics and Physics, University of Science and Technology Beijing, Beijing, 100083, China. Correspondence and requests for materials should be addressed to H.-R.W. (email: hrwei@ustb.edu.cn)
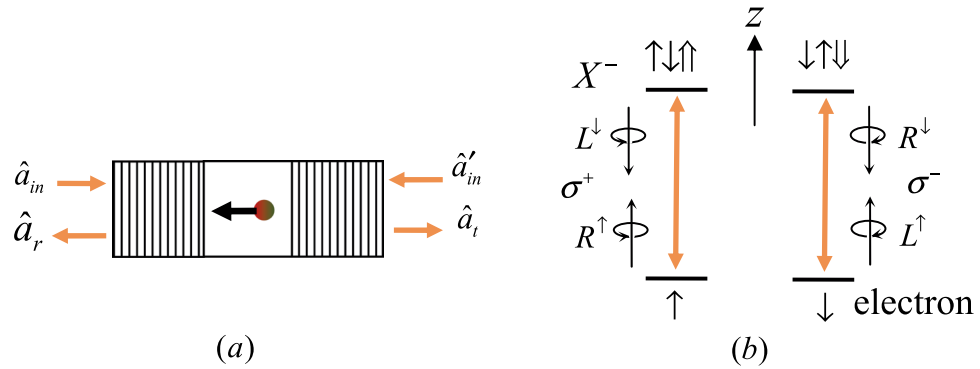
Figure 1. (**a**) A schematic diagram of the quantum dot-cavity coupled system. (**b**) Schematic description of the spin-dependent optical transition rules. $|L^{\uparrow}\rangle$ ($|L^{\downarrow}\rangle$) and $|R^{\uparrow}\rangle$ ($|R^{\downarrow}\rangle$) represent the left- and right-handed circularly polarized photons parallelled (antiparallelled) with the growth axis, respectively. $|\uparrow\rangle$ and $|\downarrow\rangle$ represent the electron spin states with $\left|\pm\frac{1}{2}\right\rangle$, respectively. $|\Uparrow\rangle$ and $|\Downarrow\rangle$ represent the heavy-hole spin states with $\left|\pm\frac{3}{2}\right\rangle$, respectively.

and such emitter was experimentally demonstrated in 2011 and 2016, respectively[37,38]. Based on QD-emitter, Bonato et al.[39], Deng et al.[40], and Wang et al.[41] proposed schemes for implementing hybrid, electronic, and photonic quantum computing gate. Other applications such as hyper-parallel universal gates[42,43], repeater[44], photonic transistor[45], router[46], entanglement and hyper-entanglement states analysis[47], purification and distillation[48] and so on have been proposed. The side leakage and the imperfect birefringent propagation of the incident photon, which reduce the fidelity and efficiency of the devices, are not taken into account in above schemes.

Hyperentanglement is a potential resource in QIP, and it can be used for some important applications[49]. In 2016, Li and Deng[50] proposed a scheme for generating error-rejecting Bell states assisted by QD-single-side-cavity platforms. Hyper-parallel CNOT and Toffoli gates with perfect input-output relations have been proposed[42,51]. In this paper, we propose a deterministic scheme for efficiently implementing self-error-rejecting optical hyper-parallel Toffoli gate on polarization and spatial DOFs, without using any auxiliary polarization DOFs. The imperfect birefringent propagations of the incident photons induced by side leakage and the limited QD-cavity coupling strength are taken into account. Our practical scheme has some characters. First, it is a practical proposal, and the inevitable imperfect performances can be detected by single-photon detectors. Second, the strong coupling limitations can be avoided and the proposal allows low-Q cavities. Third, the near-unity fidelity can be achieved in principle. Fourth, the success of the deterministic scheme can be heralded by the single-photon detectors. Fifth, the efficiency of the scheme can be further improved by repeating the operation processes when the detectors are clicked. Sixth, compared to the traditional one, our proposal reduces the noise effect, operation time, and quantum resources by a half.

Results

The optical property of a QD-microcavity platform.
Now we consider a singly charged QD [e.g., a self-assembled in(Ga)As QD or GaAs QD] incorporated into the center of a double-sided optical resonator with tens to hundreds GHz (high speed)[29,52]. As shown in Fig. 1, the QD is confined in the center of the double-sided microcavity. When an excess electron is injected, a negative charged exciton (X^-) consisting of two electrons and a hole is created by optical excitation[53]. Here, both the ground states (the electron spin states) and the excited states (the spin states of the X^-) are twofold degenerate due to the Kramer's theorem[54,55]. There are two spin-dependent transition interacting with circularly polarized lights in QD-doubled-sided unite[56] due to the Pauli's exclusion principle and the conservation of the total spin angular momentum. The $s_z = +1$ polarized photon (marked by $|L^{\downarrow}\rangle$ and $|R^{\uparrow}\rangle$) and $s_z = -1$ polarized photon (marked by $|L^{\uparrow}\rangle$ and $|R^{\downarrow}\rangle$) only couple the transition $|\uparrow\rangle \rightarrow |\uparrow\downarrow\Uparrow\rangle$ and $|\downarrow\rangle \rightarrow |\downarrow\uparrow\Downarrow\rangle$, respectively, and then the incident photons are reflected by the cavity. Otherwise, the photons can not couple to the QD and feel the cold cavity ($g = 0$), and then it is transmitted through the cavity. Upon reflection, both the polarization and the propagation direction of the incident photon will be flipped. Whereas, the spin of the electron remains unchanged upon both the reflection and transmission. Here, $|R\rangle$ and $|L\rangle$ denote the right- and left-handed circularly polarized light, respectively. The superscripts $|\uparrow\rangle$ and $|\downarrow\rangle$ of $|M^{\uparrow}\rangle$ and $|M^{\downarrow}\rangle$ indicate the propagation direction of the M-polarized photon parallel and antiparallel to the z axis (the growth and optical axis). $|\Uparrow\rangle$ and $|\Downarrow\rangle$ represent the heavy-hole spin states with $\left|\pm\frac{3}{2}\right\rangle$, respectively. $|\uparrow\rangle$ and $|\downarrow\rangle$ represent the electron spin states with $\left|\pm\frac{1}{2}\right\rangle$, respectively.

The reflection and the transmission coefficients of double-sided cavity can be obtained from the Heisenberg equations of motion for the cavity field operator $\hat{a}$, the (X^-) dipole operator σ_- and the input-output relations between the output fields $\hat{a}_r$, $\hat{a}_t$, and the input fields $\hat{a}_{in}$, $\hat{a}'_{in}$[57],

$$\frac{d\hat{a}}{dt} = -\left[i(\omega_c - \omega) + \kappa + \frac{\kappa_s}{2}\right]\hat{a} - g\sigma_- - \sqrt{\kappa}\,\hat{a}_{in} - \sqrt{\kappa}\,\hat{a}'_{in} + \hat{H},$$

$$\frac{d\sigma_-}{dt} = -\left[i(\omega_{X^-} - \omega) + \frac{\gamma}{2}\right]\sigma_- - g\sigma_z\hat{a} + \hat{G},$$

$$\hat{a}_r = \hat{a}_{in} + \sqrt{\kappa}\,\hat{a},$$

$$\hat{a}_t = \hat{a}'_{in} + \sqrt{\kappa}\,\hat{a}. \tag{1}$$

where ω, ω_c, and ω_{X^-} denote the frequencies of the external field (probe photon), the cavity mode, and the X^- transition, respectively. g denotes the cavity coupling strength between X^- and cavity mode. $\gamma/2$, κ, and $\kappa_s/2$ denote the decay rates of the X^- dipole, the cavity field, and the leaky mode (side leakage), respectively. $\hat{H}$ and $\hat{G}$ are the noise operators.

In the approximation of a weak excitation condition with (X^-) predominantly staying in the ground state, and taking $\langle\sigma_z\rangle \approx -1$ and $\sigma_z\hat{a} = -\hat{a}$, one can find that the reflection and the transmission coefficients of the (X^-) cavity system can be expressed as[29,58],

$$r(\omega) = 1 + t(\omega), \quad t(\omega) = \frac{-\kappa\left[i(\omega_{X^-} - \omega) + \frac{\gamma}{2}\right]}{\left[i(\omega_{X^-} - \omega) + \frac{\gamma}{2}\right]\left[i(\omega_c - \omega) + \kappa + \frac{\kappa_s}{2}\right] + g^2}. \tag{2}$$

For convenience to discussions, we consider the cavity mode is resonant with optical transition of the QD, i.e., $\omega_c = \omega_{X^-} = \omega_0$, and then the interaction between the incident photon and the cavity can be summarized as

$$|R^\uparrow\uparrow\rangle \to r|L^\downarrow\uparrow\rangle, \quad |L^\downarrow\uparrow\rangle \to r|R^\uparrow\uparrow\rangle,$$
$$|R^\uparrow\downarrow\rangle \to t_0|R^\uparrow\downarrow\rangle, \quad |L^\downarrow\downarrow\rangle \to t_0|L^\downarrow\downarrow\rangle,$$
$$|R^\downarrow\downarrow\rangle \to r|L^\uparrow\downarrow\rangle, \quad |L^\uparrow\downarrow\rangle \to r|R^\downarrow\downarrow\rangle,$$
$$|R^\downarrow\uparrow\rangle \to t_0|R^\downarrow\uparrow\rangle, \quad |L^\uparrow\uparrow\rangle \to t_0|L^\uparrow\uparrow\rangle. \tag{3}$$

However, in the practical working, the imperfect birefringence of the cavity, caused by the nonzero photon bandwidth, the mismatch and the finite coupling rate between the photon and the cavity mode, makes Eq. (3) changed as

$$|R^\uparrow\uparrow\rangle \to r|L^\downarrow\uparrow\rangle + t|R^\uparrow\uparrow\rangle, \quad |L^\downarrow\uparrow\rangle \to r|R^\uparrow\uparrow\rangle + t|L^\downarrow\uparrow\rangle,$$
$$|R^\uparrow\downarrow\rangle \to t_0|R^\uparrow\downarrow\rangle + r_0|L^\downarrow\downarrow\rangle, \quad |L^\downarrow\downarrow\rangle \to t_0|L^\downarrow\downarrow\rangle + r_0|R^\uparrow\downarrow\rangle,$$
$$|R^\downarrow\downarrow\rangle \to r|L^\uparrow\downarrow\rangle + t|R^\downarrow\downarrow\rangle, \quad |L^\uparrow\downarrow\rangle \to r|R^\downarrow\downarrow\rangle + t|L^\uparrow\downarrow\rangle,$$
$$|R^\downarrow\uparrow\rangle \to t_0|R^\downarrow\uparrow\rangle + r_0|L^\uparrow\uparrow\rangle, \quad |L^\uparrow\uparrow\rangle \to t_0|L^\uparrow\uparrow\rangle + r_0|R^\downarrow\uparrow\rangle. \tag{4}$$

Here the reflection coefficient r (r_0) and the transmission coefficient t (t_0) are described by Eq. (2) with $g \neq 0$ ($g = 0$).

In the following, we introduce our practical proposal for implementing emission-based three-photon hyper-parallel controlled-controlled-phase-flip gate, step by step. It is known that Toffoli gate is equivalent to the controlled-controlled-phase-flip gate upon to two Hadamard gates acting on the target qubit.

Three-photon Toffoli gate acting on polarization DOF. Let us first introduce the performance of the key building block in our scheme. As shown in Fig. 2(a), the circularly polarizing beam splitter, PBS₁, transmits the input R-polarized wave packet into spatial mode k_1 and reflects the L-polarized wave packet into spatial mode i_1. Before and after the wave packets emitted from spatial mode k_1 and k_2 interact with the QD, Hadamard operations are performed on the spatial mode and the polarized mode respectively. The performance of the polarized-(spatial-) Hadamard operation can be written as

$$H = \frac{1}{\sqrt{2}}\begin{pmatrix} 1 & 1 \\ 1 & -1 \end{pmatrix}. \tag{5}$$

in the basis $\{|R\rangle, |L\rangle\}$ ($\{|k_1\rangle, |k_2\rangle\}$). Here, the spatial- and polarized- Hadamard transformation, H_s and H_p, can be implemented by using a nonpolarizing beam splitter (BS) and a half wave plate oriented at 22.5°, respectively. Therefore, operations (PBS₁ → BS → H_{p1}, H_{p2} → QD → H_{p1}, H_{p2} → BS) make the joint state

$$|\phi_1\rangle = (\alpha|R\rangle + \beta|L\rangle)(\gamma|\uparrow\rangle + \delta|\downarrow\rangle) \tag{6}$$

become

$$|\phi_2\rangle = \alpha\gamma(r + t_0)|R^{k_1}\rangle|\uparrow\rangle + \alpha\gamma(t - t_0)|L^{k_2}\rangle|\uparrow\rangle + \alpha\delta(r + t_0)|R^{k_1}\rangle|\downarrow\rangle$$
$$-\alpha\delta(t - t_0)|L^{k_2}\rangle|\downarrow\rangle + \beta\gamma|L^{i_1}\rangle|\uparrow\rangle + \beta\delta|L^{i_1}\rangle|\downarrow\rangle. \tag{7}$$

Subsequently, the bit-flip operation X, which can be implemented by using a half wave plate oriented at 45°, is performed on the wave packet emitted from the spatial mode k_2. The wave packet emitted from the spatial mode
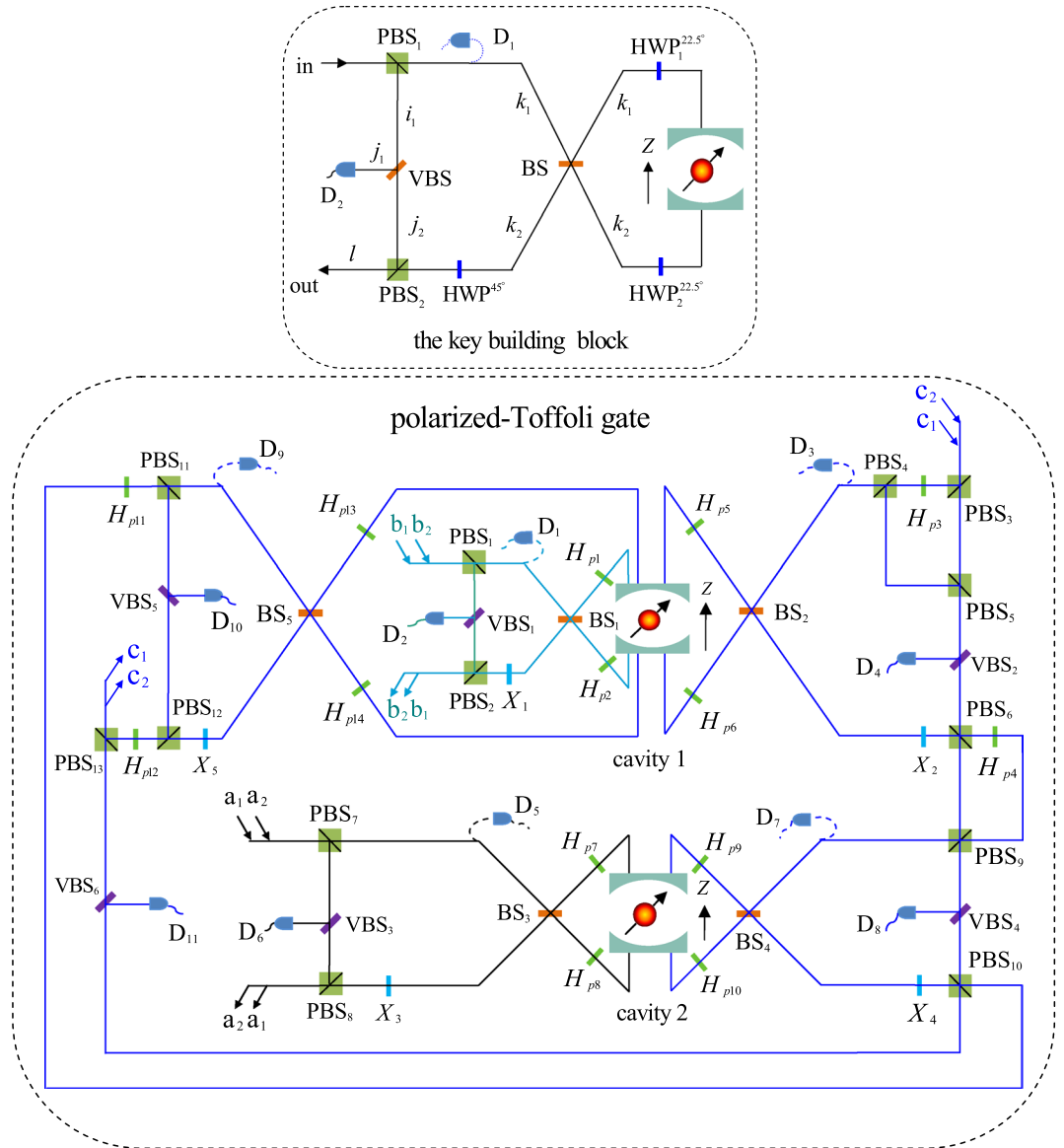
Figure 2. A schematic diagram for implementing a polarized-Toffoli gate assisted by double-sided microcavities. PBS_j ($j = 1, \ldots, 13$), a circularly polarizing beam splitter, which is used to transmit the R-polarized wave packets and reflect the L-polarized wave packets. BS_j ($j = 1, \ldots 5$), balanced nonpolarizing beam splitter, transforms the input modes as $k_1 \rightarrow (k_1 + k_2)/\sqrt{2}, k_2 \rightarrow (k_1 - k_2)/\sqrt{2}$. VBS_j ($j = 1, \ldots, 6$), an adjustable beam splitter with transmission coefficient $t - t_0$ and reflection coefficient $\sqrt{1 - (t - t_0)^2}$. D_i ($i = 1, 2, \ldots, 11$), a single photon detector. H_{pj} ($j = 1, 2, \ldots, 14$) represents a Hadamard operation on polarization, and it can be completed by using a half wave plate rotating at 22.5°. X_j ($j = 1, 2, \ldots, 5$) represents a bit-flip operation on polarization, and it can completed by using a half wave plate rotating at 45°.

i_1 passes through the adjustable beam splitter, VBS, with transmission coefficient $t - t_0$ and reflection coefficient $\sqrt{1 - (t - t_0)^2}$. And then, the wave packets emitted from the spatial mode k_2 and j_2 arrive at PBS_2, simultaneously. Therefore, X, VBS, and PBS_2 make Eq. (7) changed as

$$
\begin{aligned}
|\phi_3\rangle = & \ \alpha\gamma(t - t_0)|R^{k_2}\rangle|\uparrow\rangle - \alpha\delta(t - t_0)|R^{k_2}\rangle|\downarrow\rangle \\
& + \beta\gamma(t - t_0)|L^{j_2}\rangle|\uparrow\rangle + \beta\delta(t - t_0)|L^{j_2}\rangle|\downarrow\rangle \\
& + \alpha\gamma(r + t_0)|R^{k_1}\rangle|\uparrow\rangle + \alpha\delta(r + t_0)|R^{k_1}\rangle|\downarrow\rangle \\
& + \beta\gamma\sqrt{1 - (t - t_0)^2}|L^{j_1}\rangle|\uparrow\rangle \\
& + \beta\delta\sqrt{1 - (t - t_0)^2}|L^{j_1}\rangle|\downarrow\rangle.
\end{aligned}
\tag{8}
$$

If detectors D_1 and D_2 are not clicked, the state of the system in Eq. (8) is collapsed into the desired state

$$|\phi_4\rangle = \alpha\gamma(t-t_0)|R^l\rangle|\uparrow\rangle - \alpha\delta(t-t_0)|R^l\rangle|\downarrow\rangle$$
$$+\beta\gamma(t-t_0)|L^l\rangle|\uparrow\rangle + \beta\delta(t-t_0)|L^l\rangle|\downarrow\rangle. \tag{9}$$

From Eqs (5–9), when the detectors are not clicked, the transformation of the building block composed of PBS$_1$, PBS$_2$, BS, VBS, H_{p1}, H_{p2}, QD, X, D_1, and D_2, can be written as

$$U_{block} = (t-t_0)\begin{pmatrix} 1 & 0 & 0 & 0 \\ 0 & -1 & 0 & 0 \\ 0 & 0 & 1 & 0 \\ 0 & 0 & 0 & 1 \end{pmatrix}, \tag{10}$$

in the basis $\{|R\uparrow\rangle, |R\downarrow\rangle, |L\uparrow\rangle, |L\downarrow\rangle\}$. The efficiency of the key building block can be further improved by repeating the operation processes when the detectors are clicked.

Now we introduce the performance of our polarized-Toffoli gate, step by step. As shown in Fig. 2(b), suppose that the initial states of gate photons a, b, and c are prepared as $|\varphi_a\rangle$, $|\varphi_b\rangle$, $|\varphi_c\rangle$, respectively. Electron mediums 1 and 2 are initially prepared in the states $|\downarrow_1\rangle$ and $|\downarrow_2\rangle$, respectively. Here,

$$|\varphi_a\rangle = |\varphi_a\rangle_p \otimes |\varphi_a\rangle_s, \quad |\varphi_b\rangle = |\varphi_b\rangle_p \otimes |\varphi_b\rangle_s, \quad |\varphi_c\rangle = |\varphi_c\rangle_p \otimes |\varphi_c\rangle_s, \tag{11}$$

with

$$|\varphi_a\rangle_p = \alpha_1|R_1\rangle + \alpha_2|L_1\rangle, \quad |\varphi_b\rangle_p = \beta_1|R_2\rangle + \beta_2|L_2\rangle,$$
$$|\varphi_c\rangle_p = \gamma_1|R_3\rangle + \gamma_2|L_3\rangle, \quad |\varphi_a\rangle_s = \epsilon_1|a_1\rangle + \epsilon_2|a_2\rangle,$$
$$|\varphi_b\rangle_s = \varepsilon_1|b_1\rangle + \varepsilon_2|b_2\rangle, \quad |\varphi_c\rangle_s = \zeta_1|c_1\rangle + \zeta_2|c_2\rangle. \tag{12}$$

Where a_1 and a_2 (b_1, b_2 or c_1, c_2) represent the two spatial modes of the photon a (b or c). α_1, α_2, β_1, β_2, γ_1, γ_2, ϵ_1, ϵ_2, ε_1, ε_2, ζ_1, and ζ_2 are complex coefficients satisfying $|\alpha_1|^2 + |\alpha_2|^2 = 1$, $|\beta_1|^2 + |\beta_2|^2 = 1$, $|\gamma_1|^2 + |\gamma_2|^2 = 1$, $|\varepsilon_1|^2 + |\varepsilon_2|^2 = 1$, $|\epsilon_1|^2 + |\epsilon_2|^2 = 1$, and $|\zeta_1|^2 + |\zeta_2|^2 = 1$.

First, photon b in the spatial modes b_1 and b_2 is injected. Before and after photon b passes through the building block composed of PBS$_1$, PBS$_2$, VBS$_1$, BS$_1$, H_{p1}, H_{p2}, QD, X_1, D_1, and D_2, Hadamard operations, H_{e1} and H_{e2}, are performed on the QD$_1$ with a single photon, or an ultrafast ps or fs $\left(\frac{\pi}{2}\right)_y$ optical pulse from the cavity side[34,36,59].

When detectors D_1 and D_2 are not clicked, the above operations ($H_{e1} \rightarrow$ building block $\rightarrow H_{e2}$) transform the system composed of photon a, b, c, and QD$_1$ and QD$_2$ from the initial state $|\varphi_0\rangle$ into $|\varphi_1\rangle$. Here,

$$|\varphi_0\rangle = |\varphi_a\rangle_p \otimes |\varphi_a\rangle_s \otimes |\varphi_b\rangle_p \otimes |\varphi_b\rangle_s \otimes |\varphi_c\rangle_p \otimes |\varphi_c\rangle_s \otimes |\downarrow_1\rangle \otimes |\downarrow_2\rangle, \tag{13}$$

$$|\varphi_1\rangle = (t-t_0)(\alpha_1|R_1\rangle + \alpha_2|L_1\rangle)(\beta_1|R_2\uparrow_1\rangle + \beta_2|L_2\downarrow_1\rangle)(\gamma_1|R_3\rangle$$
$$+\gamma_2|L_3\rangle)|\downarrow_2\rangle \otimes |\varphi_a\rangle_s \otimes |\varphi_b\rangle_s \otimes |\varphi_c\rangle_s. \tag{14}$$

Second, photon c in spatial modes c_1 and c_2 is injected and arrives at PBS$_3$. PBS$_3$ transmits the R_3-polarized wave packet to PBS$_5$ and reflects the L_3-polarized wave packet into the building block composed of PBS$_4$, VBS$_2$, BS$_2$, H_{p5}, H_{p6}, QD$_1$, X_2, PBS$_6$, D_3, and D_4. Before and after the wave packets interact with the block, Hadamard operations, H_{p3} and H_{p4}, are performed on it, respectively. When $D_{1,...,4}$ are not clicked, operations (PBS$_3 \rightarrow$ PBS$_5 \rightarrow H_{p3} \rightarrow$ building block $\rightarrow H_{p4}$) make $|\varphi_1\rangle$ become

$$|\varphi_2\rangle = (t-t_0)^2(\alpha_1|R_1\rangle + \alpha_2|L_1\rangle)(\beta_1\gamma_1|R_2R_3\uparrow_1\rangle + \beta_1\gamma_2|R_2L_3\uparrow_1\rangle$$
$$+\beta_2\gamma_1|L_2R_3\downarrow_1\rangle - \beta_2\gamma_2|L_2R_3\downarrow_1\rangle))|\downarrow_2\rangle \otimes |\varphi_a\rangle_s \otimes |\varphi_b\rangle_s \otimes |\varphi_c\rangle_s. \tag{15}$$

Third, photon a in the spatial modes a_1 or a_2 is launched into the building block composed of PBS$_7$, VBS$_3$, BS$_3$, H_{p7}, H_{p8}, QD$_2$, X_3, PBS$_8$, D_5, and D_6. Before and after the wave packet interacts with the block, H_{e3} and H_{e4} are performed on QD$_2$, respectively. When $D_{1,...,6}$ are not clicked, operations ($H_{e3} \rightarrow$ building block $\rightarrow H_{e4}$) make $|\varphi_2\rangle$ changed as

$$|\varphi_3\rangle = (t-t_0)^3(\alpha_1|R_1\uparrow_2\rangle + \alpha_2|L_1\downarrow_2\rangle)(\beta_1\gamma_1|R_2R_3\uparrow_1\rangle + \beta_1\gamma_2|R_2L_3\uparrow_1\rangle$$
$$+\beta_2\gamma_1|L_2R_3\downarrow_1\rangle - \beta_2\gamma_2|L_2R_3\downarrow_1\rangle) \otimes |\varphi_a\rangle_s \otimes |\varphi_b\rangle_s \otimes |\varphi_c\rangle_s. \tag{16}$$

Fourth, photon c is leaded into the building block composed of PBS$_9$, VBS$_4$, BS$_4$, H_{p9}, H_{p10}, QD$_2$, X_4, PBS$_{10}$, D_7, and D_8. If $D_{1,...,8}$ are not clicked, the joint state is collapsed into

$$|\varphi_4\rangle = (t-t_0)^4[\alpha_1|R_1\uparrow_2\rangle(\beta_1\gamma_1|R_2R_3\uparrow_1\rangle + \beta_1\gamma_2|R_2L_3\uparrow_1\rangle$$
$$+\beta_2\gamma_1|L_2R_3\downarrow_1\rangle - \beta_2\gamma_2|L_2R_3\downarrow_1\rangle) + \alpha_2|L_1\downarrow_2\rangle(\beta_1\gamma_1|R_2R_3\uparrow_1\rangle$$
$$+\beta_1\gamma_2|R_2L_3\uparrow_1\rangle + \beta_2\gamma_1|L_2R_3\downarrow_1\rangle$$
$$+\beta_2\gamma_2|L_2R_3\downarrow_1\rangle)] \otimes |\varphi_a\rangle_s \otimes |\varphi_b\rangle_s \otimes |\varphi_c\rangle_s. \tag{17}$$

Fifth, after photon c passes through VBS_6 and the building block composed of PBS_{11}, VBS_5, BS_5, H_{p13}, H_{p14}, QD_1, X_5, PBS_{12}, D_9, and D_{10}, the desired wave packets are mixed at PBS_{13}. If $D_{1,\ldots,11}$ are not clicked, the state of the system is then becoming

$$
\begin{aligned}
|\varphi_5\rangle = & (t - t_0)^5 \left[\alpha_1 | R_1 \uparrow_2 \rangle \, (\beta_1 \gamma_1 | R_2 R_3 \uparrow_1 \rangle \right. \\
& + \beta_1 \gamma_2 | R_2 L_3 \uparrow_1 \rangle + \beta_2 \gamma_1 | L_2 R_3 \downarrow_1 \rangle \\
& + \beta_2 \gamma_2 | L_2 L_3 \downarrow_1 \rangle) + \alpha_2 | L_1 \downarrow_2 \rangle \, (\beta_1 \gamma_1 | R_2 R_3 \uparrow_1 \rangle \\
& + \beta_1 \gamma_2 | R_2 L_3 \uparrow_1 \rangle + \beta_2 \gamma_1 | L_2 R_3 \downarrow_1 \rangle \\
& \left. - \beta_2 \gamma_2 | L_2 L_3 \downarrow_1 \rangle) \right] \otimes |\varphi_a\rangle_s \otimes |\varphi_b\rangle_s \otimes |\varphi_c\rangle_s .
\end{aligned}
\tag{18}
$$

Sixth, the QD_1 and QD_2 are measured in the basis $\{|\pm\rangle = (|\uparrow\rangle \pm |\downarrow\rangle)/\sqrt{2}\}$. On detecting the QD_1 and QD_2 in the state $|+_1\rangle$ and $|+_2\rangle$, one disentangled $|\varphi_5\rangle$ into the desired outcomes of the polarized-Toffoli gate, that is,

$$
\begin{aligned}
|\varphi_6\rangle = & (t - t_0)^5 \left[\alpha_1 | R_1 \rangle \, (\beta_1 \gamma_1 | R_2 R_3 \rangle + \beta_1 \gamma_2 | R_2 L_3 \rangle \right. \\
& + \beta_2 \gamma_1 | L_2 R_3 \rangle + \beta_2 \gamma_2 | L_2 L_3 \rangle) \\
& + \alpha_2 | L_1 \rangle \, (\beta_1 \gamma_1 | R_2 R_3 \rangle + \beta_1 \gamma_2 | R_2 L_3 \rangle \\
& \left. + \beta_2 \gamma_1 | L_2 R_3 \rangle - \beta_2 \gamma_2 | L_2 L_3 \rangle) \right] \otimes |\varphi_a\rangle_s \otimes |\varphi_b\rangle_s \otimes |\varphi_c\rangle_s .
\end{aligned}
\tag{19}
$$

As for the $|+_1\rangle$ and $|-_2\rangle$ case, classical feed-forward single-qubit operations $\sigma_z = |R\rangle \langle R| - |L\rangle \langle L|$, which can be implemented by using half wave plate oriented at 0°, are performed on the outing photon a to lead the outcomes to the desired state described by Eq. (19). As for the $|-_1\rangle$ and $|+_2\rangle$ case, σ_zs are performed on the outing photon b. As for the $|-_1\rangle$ and $|-_2\rangle$ case, σ_zs are performed on the outing photon b and a, respectively.

Putting all the pieces together, one can see that Fig. 2(b) can deterministically implement an error-rejecting three-photon polarized-Toffoli gate in a heralded way, without any influence on their spatial mode quantum states.

Three-photon Toffoli gate acting on spatial DOF.

Up to now, we have discussed the implementation of the error-rejecting polarized-Toffoli gate without any influence on their spatial mode quantum states. In order to implement a hyper-parallel Toffoli gate performing controlled-controlled-NOT operations on the polarization and spatial DOFs, independently, a scheme for implementing error-rejecting three-photon spatial-Toffoli gate without any negative influence on their polarization states will be designed in this subsection.

The scheme we designed for implementing the spatial-Toffoli gate without influence on their polarization states is depicted by Fig. 3, and it can be completed by six steps. The three photons a, b, and c are initially prepared in the arbitrary product states with polarization and spatial DOFs (see Eq. (11)). QD_1 and QD_2 are prepared in the states $|\uparrow_1\rangle$ and $|\downarrow_2\rangle$, respectively.

First, the photon b is injected. The wave packets emitted from the spatial mode b_1 arrive at VBS_1 with transmission coefficient $t - t_0$ and reflection coefficient $\sqrt{1 - (t - t_0)^2}$. While the ones emitted from the spatial mode b_2 arrive at PBS_1, and PBS_1 transmits the R-polarized wave packet to the right round composed of BS_2, H_{p3}, H_{p4}, QD_1 and reflects the L-polarized wave packet to the left round composed of X_1, BS_1, H_{p1}, H_{p2}, QD_1, X_2. Here the two rounds complete the transformations

$$
\begin{aligned}
|R \uparrow\rangle &\xrightarrow{\text{rounds}} (t - t_0)|L \uparrow\rangle, \quad |R \downarrow\rangle \xrightarrow{\text{rounds}} -(t - t_0)|L \downarrow\rangle, \\
|L \uparrow\rangle &\xrightarrow{\text{rounds}} (t - t_0)|R \uparrow\rangle, \quad |L \downarrow\rangle \xrightarrow{\text{rounds}} -(t - t_0)|R \downarrow\rangle.
\end{aligned}
\tag{20}
$$

It is noted that before and after the wave packets interact with QD_1, H_es are performed on QD_1, respectively. Therefore, when D_1 and D_2 are not clicked, operations (VBS_1, $PBS_1 \to BS_2 \to H_{p3}$, $H_e \to QD_1 \to H_{p4}$, $H_e \to PBS_2$ and VBS_1, $PBS_1 \to X_1 \to BS_1 \to H_{p1}$, $H_e \to QD_1 \to H_{p2}$, $H_e \to X_2 \to PBS_2$) transform the system composed of photons a, b, c and QD_1, QD_2 from $|\psi_0\rangle = |\varphi_a\rangle \otimes |\varphi_b\rangle \otimes |\varphi_c\rangle \otimes |\uparrow_1\rangle \otimes |\downarrow_2\rangle$ into

$$
\begin{aligned}
|\psi_1\rangle = & (t - t_0) \, (\epsilon_1 |a_1\rangle + \epsilon_2 |a_2\rangle) \, (\varepsilon_1 |b_1 \uparrow_1\rangle + \varepsilon_2 |b_2 \downarrow_1\rangle) \, (\zeta_1 |c_1\rangle \\
& + \zeta_2 |c_2\rangle)| \downarrow_2 \rangle \otimes |\varphi_a\rangle_p \otimes |\varphi_b\rangle_p \otimes |\varphi_c\rangle_p .
\end{aligned}
\tag{21}
$$

Second, photon c emitted from the spatial mode c_1 passes through VBS_2 with transmit $(t - t_0)^3$ and reflect $\sqrt{1 - (t - t_0)^6}$. Photon c emitted from the spatial mode c_{2D} passes through the round composed of PBS_1, X_1, H_{p1}, H_{p2}, BS_1, X_2, QD_1, PBS_2 or the round composed of PBS_1, H_{p3}, H_{p4}, BS_2, QD_1, PBS_2. Before and after the photon passes through the two rounds, Hadamard operation H_ss, which complete the transformation,

$$
|c_{2U}\rangle \to \frac{1}{\sqrt{2}}(|c_{2U}\rangle + |c_{2D}\rangle), \quad |c_{2D}\rangle \to \frac{1}{\sqrt{2}}(|c_{2U}\rangle - |c_{2D}\rangle).
\tag{22}
$$

are performed on the spatial mode of photon c by BS_1 and BS_2. It is worthy to note that after BS_3, only the wave packets emitted from the spatial mode c_{2D} interact with QD_1. When D_3 and D_4 are not clicked, $|\psi_1\rangle$ is changed as
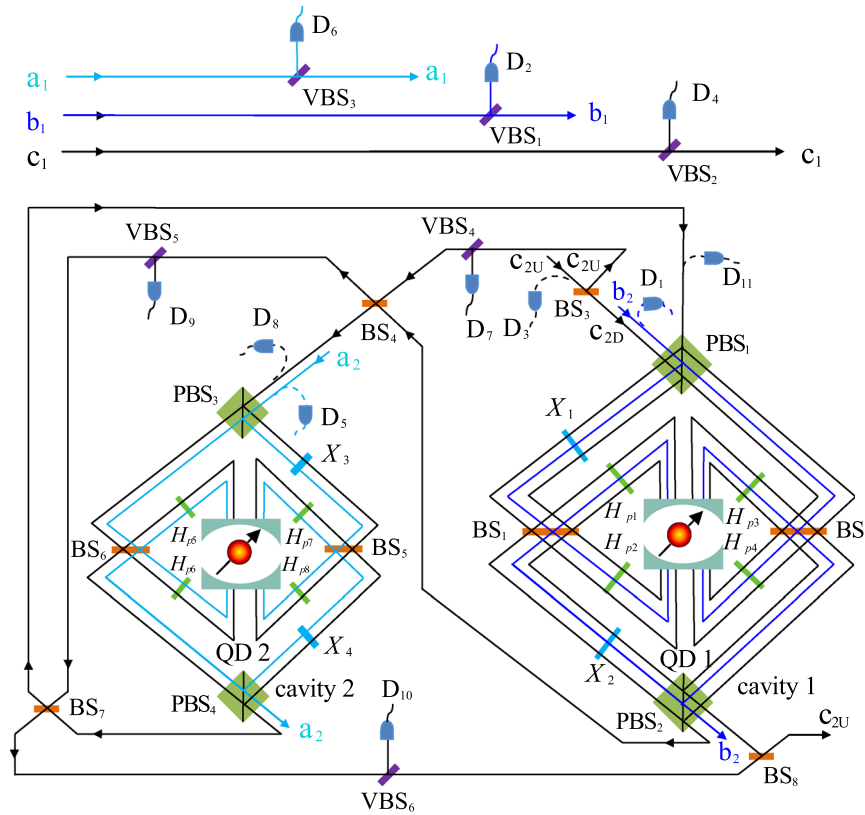
Figure 3. A schematic diagram for a spatial-Toffoli gate assisted by double-sided microcavities. Adjustable beam splitter, VBS_1 and $VBS_3, \ldots, _6$, with transmission coefficient $t - t_0$ and reflection coefficient $\sqrt{1 - (t - t_0)^2}$. VBS_2 with transmission coefficient $(t - t_0)^3$ and reflection coefficient $\sqrt{1 - (t - t_0)^6}$.

$$
\begin{aligned}
|\psi_2\rangle = {}& (\epsilon_1|a_1\rangle + \epsilon_2|a_2\rangle) \otimes |\downarrow_2\rangle \otimes |\varphi_a\rangle_p \\
& \otimes |\varphi_b\rangle_p \otimes |\varphi_c\rangle_p \otimes [(t - t_0)^4 \varepsilon_1 \zeta_1 |b_1 c_1\rangle |\uparrow_1\rangle \\
& + (t - t_0)^2 \varepsilon_1 \zeta_2 |b_1 c_{2U}\rangle |\uparrow_1\rangle + (t - t_0)^4 \varepsilon_2 \zeta_1 |b_2 c_1\rangle |\downarrow_1\rangle \\
& + (t - t_0)^2 \varepsilon_2 \zeta_2 |b_2 c_{2D}\rangle |\downarrow_1\rangle].
\end{aligned}
\tag{23}
$$

Third, photon a emitted from the spatial mode a_1 passes through VBS_3 with transmit $(t - t_0)$, and the one emitted from the spatial mode a_2 passes through the round composed of PBS_3, X_3, H_{p7}, H_{p8}, BS_5, X_4, QD_2, PBS_4 or the round composed of PBS_3, H_{p5}, H_{p6}, BS_6, QD_2, PBS_4. Here, before and after the photon passes through the two rounds, H_es are performed on QD_2, respectively. When D_5 and D_6 are not clicked, $|\psi_2\rangle$ is collapsed into the desired state

$$
\begin{aligned}
|\psi_3\rangle = {}& (\epsilon_1|a_1\rangle|\downarrow_2\rangle + \epsilon_2|a_2\rangle|\uparrow_2\rangle) \otimes |\varphi_a\rangle_p \otimes |\varphi_b\rangle_p \\
& \otimes |\varphi_c\rangle_p \otimes [(t - t_0)^5 \varepsilon_1 \zeta_1 |b_1 c_1\rangle |\uparrow_1\rangle \\
& + (t - t_0)^3 \varepsilon_1 \zeta_2 |b_1 c_{2U}\rangle |\uparrow_1\rangle + (t - t_0)^5 \varepsilon_2 \zeta_1 |b_2 c_1\rangle |\downarrow_1\rangle \\
& + (t - t_0)^3 \varepsilon_2 \zeta_2 |b_2 c_{2D}\rangle |\downarrow_1\rangle].
\end{aligned}
\tag{24}
$$

Fourth, photon c emitted from the spatial mode c_{2D} interacts with the round composed of PBS_3, X_3, H_{p7}, H_{p8}, BS_5, X_4, QD_2, PBS_4 or the round composed of PBS_3, H_{p5}, H_{p6}, BS_6, QD_2, PBS_4. From Eq. (20), one can see that when D_7, D_8, and D_9 are not clicked, the two rounds induce $|\psi_3\rangle$ to be

$$
\begin{aligned}
|\psi_4\rangle = {}& (t - t_0)^4 \{\epsilon_1|a_1\rangle|\downarrow_2\rangle [(t - t_0)\varepsilon_1 \zeta_1 |b_1 c_1\rangle |\uparrow_1\rangle + \varepsilon_1 \zeta_2 |b_1 c_{2U}\rangle |\uparrow_1\rangle \\
& + (t - t_0)\varepsilon_2 \zeta_1 |b_2 c_1\rangle |\downarrow_1\rangle - \varepsilon_2 \zeta_2 |b_2 c_{2D}\rangle |\downarrow_1\rangle] \\
& + \epsilon_2|a_2\rangle|\uparrow_2\rangle [(t - t_0)\varepsilon_1 \zeta_1 |b_1 c_1\rangle |\uparrow_1\rangle \\
& + \varepsilon_1 \zeta_2 |b_1 c_{2U}\rangle |\uparrow_1\rangle + (t - t_0)\varepsilon_2 \zeta_1 |b_2 c_1\rangle |\downarrow_1\rangle \\
& + \varepsilon_2 \zeta_2 |b_2 c_{2D}\rangle |\downarrow_1\rangle]\} \\
& \otimes |\varphi_a\rangle_p \otimes |\varphi_b\rangle_p \otimes |\varphi_c\rangle_p.
\end{aligned}
\tag{25}
$$

Fifth, after wave packets emitted from the spatial c_{2U} and c_{2D} are mixed at BS_7, the wave packet emitted from c_{2U} passes through the block composed of PBS_1, PBS_2, X_1, X_2, BS_1, BS_2, H_{p1}, H_{p2}, H_{p3}, and H_{p4}, and then they are mixed with the wave packet emitted from c_{2D} passing through the VBS_6 and BS_8. When D_9, D_{10} and D_{11} are not clicked, one can see that $|\psi_4\rangle$ is collapsed into the desired state

$$
\begin{aligned}
|\psi_5\rangle = {} & (t - t_0)^5 \{\epsilon_1 |a_1\rangle |\downarrow_2\rangle [\varepsilon_1 \zeta_1 |b_1 c_1\rangle |\uparrow_1\rangle \\
& + \varepsilon_1 \zeta_2 |b_1 c_{2U}\rangle |\uparrow_1\rangle + \varepsilon_2 \zeta_1 |b_2 c_1\rangle |\downarrow_1\rangle \\
& + \varepsilon_2 \zeta_2 |b_2 c_{2U}\rangle |\downarrow_1\rangle] \\
& + \epsilon_2 |a_2\rangle |\uparrow_2\rangle [\varepsilon_1 \zeta_1 |b_1 c_1\rangle |\uparrow_1\rangle + \varepsilon_1 \zeta_2 |b_1 c_{2U}\rangle |\uparrow_1\rangle \\
& + \varepsilon_2 \zeta_1 |b_2 c_1\rangle |\downarrow_1\rangle - \varepsilon_2 \zeta_2 |b_2 c_{2U}\rangle |\downarrow_1\rangle]\} \otimes |\varphi_a\rangle_p \otimes |\varphi_b\rangle_p \otimes |\varphi_c\rangle_p.
\end{aligned}
\tag{26}
$$

Sixth, we measure the QD_1 and QD_2 in the basis $\{|\pm\rangle = (|\uparrow\rangle \pm |\downarrow\rangle)/\sqrt{2}\}$. If the outcomes of the QD_1 and QD_2 are $|+_1\rangle$ and $|+_2\rangle$, respectively, and then the desired performance is completed. As for the $|+_1\rangle$ and $|-_2\rangle$ case, phase shifter $e^{i\pi}$, which completes the transformation $|R\rangle \rightarrow -|R\rangle$ and $|L\rangle \rightarrow -|L\rangle$, is performed on the spatial mode a_1 to complete the spatial-Toffoli gate. As for the $|-_1\rangle$ and $|+_2\rangle$ case, phase shifter $e^{i\pi}$ is performed on the spatial mode b_2. As for the $|-_1\rangle$ and $|-_2\rangle$ case, phase shifter $e^{i\pi}$s are performed on the spatial mode a_1 and b_2, respectively. That is to say, measurement and the classical feed-forward single-qubit operations make $|\psi_5\rangle$ become

$$
\begin{aligned}
|\psi_6\rangle = {} & (t - t_0)^5 \{\epsilon_1 |a_1\rangle [\varepsilon_1 \zeta_1 |b_1 c_1\rangle + \varepsilon_1 \zeta_2 |b_1 c_{2U}\rangle \\
& + \varepsilon_2 \zeta_1 |b_2 c_1\rangle + \varepsilon_2 \zeta_2 |b_2 c_{2U}\rangle] \\
& + \epsilon_2 |a_2\rangle [\varepsilon_1 \zeta_1 |b_1 c_1\rangle + \varepsilon_1 \zeta_2 |b_1 c_{2U}\rangle \\
& + \varepsilon_2 \zeta_1 |b_2 c_1\rangle - \varepsilon_2 \zeta_2 |b_2 c_{2U}\rangle]\} \\
& \otimes |\varphi_a\rangle_p \otimes |\varphi_b\rangle_p \otimes |\varphi_c\rangle_p.
\end{aligned}
\tag{27}
$$

From Eqs (20–27), one can see that the quantum circuit shown in Fig. 3 can be used to implement a robust three-photon spatial-Toffoli gate without any influence on their polarization mode quantum states in a deterministic way.

Discussion

QDs mimic the behavior of single atomic dipole-like transitions. However, unlike atoms, QDs can be easily incorporated into solid-state devices such as cavities or waveguide that enhance the light-matter interaction for scalable QIP. Moreover, the manipulation can be achieved with high-speed (up to THz). The coupling efficiency of the pillar microcavity is higher than waveguide as the pillar cavity mode is Guassian type and matches perfectly with the external laser beam. Compared to the devices via QD-double-sided emitters, the ones via QD-single-sided emitters are fragile due to the balanced reflectance, for the coupled and uncoupled cavities are necessary to get high fidelity[29]. The length and deep of the gates via QD-double-sided emitters usually are surpass the ones via QD-single-sided emitters as the maximum Faraday rotation π can be achieved in particular QD-double-sided emitter[29], whereas $\pi/2$ is for the QD-single-sided oemitter[60].

The unconstructed low theoretical lower bound for a generic traditional n-qubit gates is $\left[\frac{1}{4}(4^n - 3n - 1)\right]$ CNOT gates[61]. Up to now, the optimal cost of a traditional Toffoli gate acting on single DOF is 6 CNOT gates[12,62]. The scheme we designed for physical implementing a hyper-parallel Toffoli gate acting on two DOFs, and the essential cost of our scheme is 6 CNOT gates. Compared to the traditional one, our hyper-parallel Toffoli gate reduces the quantum resource, the operation time, and the influence of the noise by half. The previous works mainly were investigated via the optical transition rules in Eq. (3), that is, the side-leakage and the imperfect birefringence of the cavity are not taken into account[28,29,37] and $t_0 \rightarrow -1$, $r \rightarrow 1$. Our hyper-parallel Toffoli gate are constructed via Eq. (4), and the undesired performances caused by the side leakage and the imperfect birefringence are detected by the detectors. Moreover, the strong coupling limitation can be avoided in our scheme because the fidelity of our scheme is unity in principle.

In summary, we have designed a quantum circuit for implementing a heralded error-rejecting hyper-parallel Toffoli gate assisted by QD-double-sided cavities. It is a practical proposal, and the side leakage and the imperfect birefringence of the incident photons are detected. The fidelity of the present gate is always unity and the efficiency can be further improved by repeating the construction processes. In addition, our scheme overcomes the exciting strong coupling limitations, and can work in both the strong-coupling and the weak-coupling regimes. These interesting features make us believe that the present work may be useful for some practical hyper-parallel quantum information processing, including hyper-entanglement concentration[63] and purification[48], hyper-entanglement state analysis, hyper-parallel quantum repeater and so on.

Evaluation of the performance. An efficient QD-photon has been recognized as a potential building block for QIP due to their inherent scalability and mature semiconductor technology[28,29]. QDs incorporated into photonic-crystal (PC) waveguides[64,65], photonic nanowires[66], pillar microcavities[37,67,68], and photonic crystal cavities cite[69] have been achieved in experiment. In the present, the double-sided symmetric pillar cavity supports circularly polarized light, and it incorporates a negative charged QD. This type of cavity has been fabricated in experiment[68]. Some specific symmetry photonic crystal nanocavities[70] are suitable for proposal as well. Compared to weak coupling cavity-QED system, strong coupling cavity-QED system is a challenge in experiment with current technology. Fortunately, the strong coupling regime $g/(\kappa + \kappa_s) = 2.4$ ($g = 80\,\mu eV$, $\kappa + \kappa_s = 33\,\mu eV$), has been
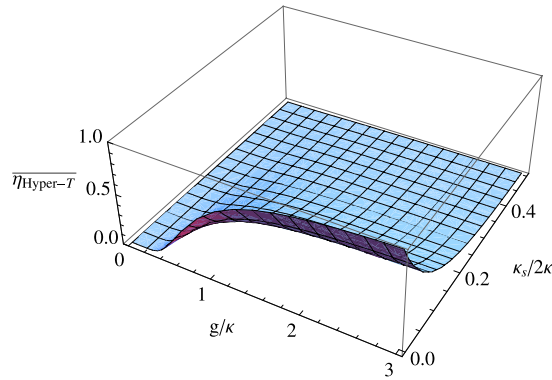
Figure 4. The average efficiency of the hyper-parallel Toffoli gate as the function of the coupling strength g/κ and side leakage κ_s/κ averaged over $[0, 2\pi]$. $\gamma = 0.1\kappa$ is taken.

demonstrated for INAs QDs in the state-of-the-art pillar microcavity recently[67,71]. The strong limitations are not necessary in our proposal because the imperfect performance caused by the strong coupling can be detected by the detector. Hu et al.[29,37] showed that the π phase shift, which is necessary for the emitter-based quantum gates, can be achieved in this particular double-sided-QD-cavity combination.

The performance of the gate can be characterized by the fidelity and efficiency. According to the arguments in result, one can find that the unity fidelity of our practical hyper-parallel Toffoli gate can be achieved in principle if the overall phase is ignored. The efficiency of the present gate depends on cavity QED parameters (g, κ, κ_s, γ), and it can be further improved by repeating the operation processes when the undesired performances are detected. Here, the efficiency is defined as the ratio between the number of the output photons to the input photons. The shape functions $\overline{\eta}$ is plotted in Fig. 4 for the average efficiency of the present gate averaged over $[0, 2\pi]$. $\gamma \sim \mu$eV caused by the the spontaneous emission and the pure dephasing is usually smaller than $\kappa + \kappa_s$ in high-quality QD-cavity samples. Here $\gamma = 0.1\kappa$, which is experimentally achieved, is taken. Figure 4 suggests that we could make high efficiency in the strong coupling regime when the side leakage κ_s/κ is small. The strong coupling QD-cavity system has been reported[67,71]. The side leakage, κ_s, can be reduced by engineering the fabrication and various cavity details such as materials, structures, size, etc.

Photon loss has no contribution to the fidelity of the gate. In realistic case, the fidelity of the emitter can be decreased by a factor[29], $F = [1 + \exp(-\Delta t/T_2^e)]/2$, due to spin decoherence. Therefore, the lower is the $\Delta t/T_2^e$, the higher is the F. Here T_2^e and Δt are the electron spin coherence time and the time interval between input photons, respectively. $T_2^e \sim \mu$s and $\Delta t \sim$ ns have been achieved in experiment[72]. The imperfect spin-selection rules, induced by the heavy-light hole mixing, reduce emitter fidelity by a few percent[73,74]. The heavy-light hole mixing depends on the kind, shape and size of the QD. The emitter fidelity can be reduced by amount of $F = [1 - \exp(-\tau/T_2)]$ caused by the QD spin dephasing, and such influence can be neglected because $T_2 \sim \mu$s and $\tau \sim$ ps have been experimentally demonstrated in the coupling regime with 10^4–10^5[75,76]. Here, τ and T_2 are the cavity photon lifetime and QD coherence time, respectively. Moreover, the technical imperfection such as photon detection events, the unbalanced PBSs, and the spatial mismatch between the cavity mode and the photon influence the success probability and the fidelity of the gate.

References

1. Grover, L. K. Quantum mechanics helps in searching for a needle in a haystack. *Phys. Rev. Lett.* **79**, 325 (1997).
2. Long, G. L. Grover algorithm with zero theoretical failure rate. *Phys. Rev. A* **64**, 022307 (2001).
3. Shor, P. W. Polynomial-time algorithms for prime factorization and discrete logarithms on a quantum computer. *SIAM (Soc. Ind. Appl. Math.) J. Stat. Comput.* **26**, 1474–1509 (1997).
4. Feynman, R. P. Simulating physics with computers. *Int. J. Theor. Phys.* **21**, 467–488 (1982).
5. Lu, Y. *et al*. Experimental digital quantum simulation of temporal-spatial dynamics of interacting fermion system. *Sci. Bull.* **60**, 241–248 (2015).
6. Xi, T. *et al*. Quantum state tomography via reduced density matrices. *Phys. Rev. Lett.* **118**, 020401 (2017).
7. Wang, X. L. *et al*. Quantum teleportation of multiple degrees of freedom of a single photon. *Nature* **518**, 516–519 (2015).
8. Sheng, Y. B., Deng, F. G. & Long, G. L. Complete hyperentangled-Bell-state analysis for quantum communication. *Phys. Rev. A* **10**, 032318 (2010).
9. Barenco, A. *et al*. Elementary gates for quantum computation. *Phys. Rev. A* **52**, 3457 (1995).
10. Liu, Y., Long, G. L. & Sun, Y. Analytic one-bit and CNOT gate constructions of general n-qubit controlled gates. *Int. J. Quantum Inf.* **6**, 447–462 (2008).
11. Guerrero, R. J. & Rojas, F. Effect of the Dzyaloshinski-Moriya term in the quantum SWAP$^\alpha$ gate produced with exchange coupling. *Phys. Rev. A* **77**, 012331 (2008).
12. Nielsen, M. A. & Chuang, I. L. *Quantum Computation and Quantum Information*. (Cambridge University, Cambridge, 2000).
13. Cory, D. G. *et al*. Experimental quantum error correction. *Phys. Rev. Lett.* **81**, 2152 (1998).
14. Yu, N. K. & Ying, M. S. Optimal simulation of Deutsch gates and the Fredkin gate. *Phys. Rev. A* **91**, 032302 (2015).
15. Dennis, E. Toward fault-tolerant quantum computation without concatenation. *Phys. Rev. A* **63**, 052314 (2001).
16. Cirac, J. I., Zoller, P., Kimble, H. J. & Mabuchi, H. Quantum state transfer and entanglement distribution among distant nodes in a quantum network. *Phys. Rev. Lett.* **78**, 3221 (1997).
17. Shi, Y. Y. Both Toffoli and controlled-not need little help to do universal quantum computation. *Quant. Inf. Comput.* **3**, 084–092 (2003).

18. Fredkin, E. & Toffoli, T. Conservative logic. *Int. J. Theor. Phys.* **21**, 219–253 (1982).
19. Knill, E., Laflamme, R. & Milburn, G. J. A scheme for efficient quantum computation with linear optics. *Nature* **409**, 46–52 (2001).
20. Feng, G. R., Xu, G. F. & Long, G. L. Experimental realization of nonadiabatic holonomic quantum computation. *Phys. Rev. Lett.* **110**, 190501 (2013).
21. Hua, M., Tao, M. J. & Deng, F. G. Universal quantum gates on microwave photons assisted by circuit quantum electrodynamics. *Phys. Rev. A* **90**, 012328 (2014).
22. van der Sar, T. *et al.* Decoherence-protected quantum gates for a hybrid solid-state spin register. *Nature* **484**, 82–86 (2012).
23. Li, H., Liu, Y. & Long, G. L. Experimental realization of single-shot nonadiabatic holonomic gates in nuclear spins. *Sci. China Phys. Mech.* **60**, 080311 (2017).
24. Zhen, X. L., Xin, T., Zhang, F. H. & Long, G. L. Experimental demonstration of concatenated composite pulses robustness to non-static errors. *Sci. China Phys. Mech.* **59**, 690312 (2016).
25. Pile, D. How many bits can a photon carry? *Nat. Photon.* **6**, 14–15 (2012).
26. Duan, L. M. & Kimble, H. J. Scalable photonic quantum computation through cavity-assisted interactions. *Phys. Rev. Lett.* **92**, 127902 (2004).
27. Gorshkov, A. V., Otterbach, J., Fleischhauer, M., Pohl, T. & Lukin, M. D. Photon-photon interactions via Rydberg blockade. *Phys. Rev. Lett.* **107**, 133602 (2011).
28. Hu, C. Y., Munro, W. J. & Rarity, J. G. Deterministic photon entangler using a charged quantum dot inside a microcavity. *Phys. Rev. B* **78**, 125318 (2008).
29. Hu, C. Y., Munro, W. J., O'Brien, J. L. & Rarity, J. G. Proposed entanglement beam splitter using a quantum-dot spin in a double-sided optical microcavity. *Phys. Rev. B* **80**, 205326 (2009).
30. Togan, E. *et al.* Quantum entanglement between an optical photon and a solid-state spin qubit. *Nature* **466**, 730–734 (2010).
31. Xiao, Y. F. & Gong, Q. Optical microcavity: from fundamental physics to functional photonics devices. *Sci. Bull.* **61**, 185–186 (2016).
32. Reiserer, A., Kalb, N., Rempe, G. & Ritter, S. A quantum gate between a flying optical photon and a single trapped atom. *Nature* **508**, 237–240 (2014).
33. Hacker, B., Welte, S., Rempe, G. & Ritter, S. A photon-photon quantum gate based on a single atom in an optical resonator. *Nature* **536**, 193–196 (2016).
34. Press, D. *et al.* Ultrafast optical spin echo in a single quantum dot. *Nat. Photon.* **4**, 367–370 (2010).
35. Stockill, R. *et al.* Quantum dot spin coherence governed by a strained nuclear environment. *Nat. Commun.* **7**, 12745 (2016).
36. Pressl, D., Ladd, T. D., Zhang, B. Y. & Yamamoto, Y. Complete quantum control of a single quantum dot spin using ultrafast optical pulses. *Nature* **456**, 218–221 (2008).
37. Androvitsaneas, P. *et al.* Charged quantum dot micropillar system for deterministic light-matter interactions. *Phys. Rev. B* **93**, 241409(R) (2016).
38. Arnold, C. *et al.* Macroscopic rotation of photon polarization induced by a single spin. *Nat. Commun.* **6**, 6236 (2015).
39. Bonato, C. *et al.* CNOT and Bell-state analysis in the weak-coupling cavity QED regime. *Phys. Rev. Lett.* **104**, 160503 (2010).
40. Wei, H. R. & Deng, F. G. Universal quantum gates for hybrid systems assisted by quantum dots inside double-sided optical microcavities. *Phys. Rev. A* **87**, 022305 (2013).
41. Wang, T. J., Zhang, Y. & Wang, C. Universal hybrid hyper-controlled quantum gates assisted by quantum dots in optical double-sided microcavities. *Laser Phys. Lett.* **11**, 025203(7pp) (2014).
42. Ren, B. C., Wei, H. R. & Deng, F. G. Deterministic photonic spatial-polarization hyper-controlled-not gate assisted by quantum dot inside one-side optical microcavity. *Laser Phys. Lett.* **10**, 095202 (2013).
43. Ren, B. C. & Deng, F. G. Hyper-parallel photonic quantum computing with coupled quantum dots. *Sci. Rep.* **4**, 4623 (2014).
44. Wang, T. J., Song, S. Y. & Long, G. L. Quantum repeater based on spatial entanglement of photons and quantum-dot spins in optical microcavities. *Phys. Rev. A* **85**, 062311 (2012).
45. Hu, C. Y. Spin-based single-photon transistor, dynamic random access memory, diodes, and routers in semiconductors. *Phys. Rev. B* **94**, 245307 (2016).
46. Hu, C. Y. Photonic transistor and router using a single quantum-dot-confined spin in a single-sided optical microcavity. *Sci. Rep.* **7**, 45582 (2017).
47. Wang, T. J., Lu, Y. & Long, G. L. Generation and complete analysis of the hyperentangled Bell state for photons assisted by quantum-dot spins in optical microcavities. *Phys. Rev. A* **86**, 042337 (2012).
48. Ren, B. C., Du, F. F. & Deng, F. G. Two-step hyperentanglement purification with the quantum-state-joining method. *Phys. Rev. A* **90**, 052309 (2014).
49. Deng, F. G., Ren, B. C. & Li, X. H. Quantum hyperentanglement and its applications in quantum information processing. *Sci. Bull.* **62**, 46–68 (2017).
50. Li, T. & Deng, F. G. Error-rejecting quantum computing with solid-state spins assisted by low-Q optical microcavities. *Phys. Rev. A* **94**, 062310 (2016).
51. Wei, H. R., Deng, F. G. & Long, G. L. Hyper-parallel Toffoli gate on three-photon system with two degrees of freedom assisted by single-sided optical microcavities. *Optics Express* **24**, 18619–18630 (2016).
52. Wang, G. Y., Ai, Q., Ren, B. C., Li, T. & Deng, F. G. Error-detected generation and complete analysis of hyperentangled Bell states for photons assisted by quantum-dot spins in double-sided optical microcavities. *Optics Express* **24**, 28444–28458 (2016).
53. Warburton, R. J. *et al.* Charged excitons in self-assembled semiconductor quantum dots. *Phys. Rev. Lett.* **79**, 5282 (1997).
54. Hansom, J. *et al.* Environment-assisted quantum control of a solid-state spin via coherent dark states. *Nat. Phys.* **10**, 725–730 (2014).
55. Urbaszek, B. *et al.* Nuclear spin physics in quantum dots: An optical investigation. *Rev. Mod. Phys.* **85**, 79–133 (2013).
56. Hu, C. Y. *et al.* Optically detected magnetic resonance of excess electrons in type-I quantum wells with a low-density electron gas. *Phys. Rev. B* **58**, R1766 (1998).
57. Walls, D. F. & Miburn, G. J. *Quantum optics*. (Springer-Verlag, Berlin, 1994).
58. An, J. H., Feng, M. & Oh, C. H. Quantum-information processing with a single photon by an input-output process with respect to low-Q cavities. *Phys. Rev. A* **79**, 032303 (2009).
59. Berezovsky, J., Mikkelsen, M. H., Stoltz, N. G., Coldren, L. A. & Awschalom, D. D. Picosecond coherent optical manipulation of a single electron spin in a quantum dot. *Science* **320**, 349–352 (2008).
60. Hofmann, H. F., Kojima, K., Takeuchi, S. & Sasaki, K. Optimized phase switching using a single-atom nonlinearity. *J. Opt. B* **5**, 218 (2003).
61. Shende, V. V., Markov, I. L. & Bullock, S. S. Minimal universal two-qubit controlled-not-based circuits. *Phys. Rev. A* **69**, 062321 (2004).
62. Shende, V. V. & Markov, I. L. On the CNOT-cost of Toffoli gates. *Quant. Inf. Comp.* **9**, 461–486 (2009).
63. Sheng, Y. B., Pan, J., Guo, R., Zhou, L. & Wang, L. Efficient N-particle W state concentration with different parity check gates. *Sci. China Phys. Mech.* **58**, 60301 (2015).
64. Lund-Hansen, T. *et al.* Experimental realization of highly efficient broadband coupling of single quantum dots to a photonic crystal waveguide. *Phys. Rev. Lett.* **101**, 113903 (2008).
65. Javadi, A. *et al.* Single-photon non-linear optics with a quantum dot in a waveguide. *Nat. Common.* **6**, 8655 (2015).
66. Claudon, J. *et al.* A highly efficient single-photon source based on a quantum dot in a photonic nanowire. *Nat. Photon.* **4**, 174–177 (2010).

67. Reithmaier, J. P. *et al*. Strong coupling in a single quantum dot-semiconductor microcavity system. *Nature* **432**, 197–200 (2004).
68. Schneider, C., Gold, P., Reitzenstein, S., Höfling, S. & Kamp, M. Quantum dot micropillar cavities with quality factors exceeding 250,000. *Appl. Phys. B* **122**, 19 (2016).
69. Yoshie, T. *et al*. Vacuum Rabi splitting with a single quantum dot in a photonic crystal nanocavity. *Nature* **432**, 200–203 (2004).
70. Vahala, K. J. Optical microcavities. *Nature* **424**, 839 (2003).
71. Reitzenstein, S. *et al*. AlAs/GaAsAlAs/GaAs micropillar cavities with quality factors exceeding 150.000. *Appl. Phys. Lett.* **90**, 251109 (2007).
72. Greilich, A. *et al*. Mode locking of electron spin coherences in singly charged quantum dots. *Science* **313**, 341–345 (2006).
73. Calarco, T., Datta, A., Fedichev, P., Pazy, E. & Zoller, P. Spin-based all-optical quantum computation with quantum dots: Understanding and suppressing decoherence. *Phys. Rev. A* **68**, 012310 (2003).
74. Bester, G., Nair, S. & Zunger, A. Pseudopotential calculation of the excitonic fine structure of million-atom self-assembled $In_{1-x}Ga_xAs$/GaAs quantum dots. *Phys. Rev. B* **67**, 161306 (2003).
75. Borri, P. *et al*. Ultralong dephasing time in InGaAs quantum dots. *Phys. Rev. Lett.* **87**, 157401 (2001).
76. Birkedal, D., Leosson, K. & Hvam, J. M. Long lived coherence in self-assembled quantum dots. *Phys. Rev. Lett.* **87**, 227401 (2001).

Acknowledgements

Author Contributions

H.R., J.Z., and N.Y. contributed equally to this work, and they wrote the manuscript text and prepared Figures 1, 2, 3 and 4. H.R. supervised the whole project.

Additional Information

Competing Interests: The authors declare that they have no competing interests.

Publisher's note: Springer Nature remains neutral with regard to jurisdictional claims in published maps and institutional affiliations.